Exchange mixing and soliton dynamics in the quantum spin chain $CsCoCl_3$

J. P. Goff and D. A. Tennant
Oxford Physics, Clarendon Laboratory, Parks Road, Oxford OX1 3PU, United Kingdom

S. E. Nagler*
Department of Physics, University of Florida, Gainseville, Florida 32611
(Received 17 May 1995)

The lowest-lying excited states in the $S=\frac{1}{2}$ one-dimensional Ising-like antiferromagnet $CsCoCl_3$ consist of domain-wall (soliton) pair states. Although the dynamical response function $S(Q,\omega)$ has been calculated for these states, it has not proved possible to explain the results of neutron scattering and Raman experiments without recourse to the introduction of extra terms in the spin Hamiltonian. We argue against the two modifications to the Hamiltonian of $CsCoCl_3$ proposed in previous papers, a staggered field term arising from a mean field approach to exchange mixing, and next-nearest-neighbor intrachain coupling, as being unphysical. Instead we derive a nearest-neighbor effective Hamiltonian, which takes account of the mixing of higher Co^{2+} ion crystal-field levels in a self-consistent manner. We also present a high-resolution inelastic neutron scattering experiment on $CsCoCl_3$, which has allowed the dispersion of the excited states across the Brillouin zone to be studied more carefully than before. These results give a direct measure of $S(Q,\omega)$ in the one-dimensional phase where there is a continuum of excited states, and in the three-dimensionally ordered phases, where weak interchain interactions split the continuum into a "Zeeman ladder" of discrete states. The predictions of our theory are found to be in quantitative agreement with experiment.

I. INTRODUCTION

$CsCoCl_3$ is of particular interest because it is a realization of one of the simplest quantum systems to exhibit soliton excitations: the $S=\frac{1}{2}$ antiferromagnetic chain with near-Ising-like exchange. Compared to other one-dimensional Hamiltonians, the Ising-like system has the advantage of being straightforward to understand mathematically, while still showing characteristic soliton-pair excitations,[1,2] a behavior encountered in the mathematically more involved XY,[3] and Heisenberg[4,5] systems. In this context $CsCoCl_3$ is worthy of detailed experimental study, and has been investigated quite extensively using NMR,[6] Raman-scattering,[7,8] and neutron-scattering techniques.[9–11] It has become apparent from these measurements that the one-dimensional antiferromagnetic Ising-like Hamiltonian cannot explain all of the data on $CsCoCl_3$ consistently, and modifications of the spin Hamiltonian for $CsCoCl_3$ have been suggested.[11–14]

In this paper we take issue with the approaches taken in Refs. 11–14, and instead propose a new form of the Hamiltonian, derived entirely from the known properties of the coupled Co^{2+} ions comprising the system. We also present high-resolution neutron-scattering measurements of the excitation continuum of $CsCoCl_3$. The inelastic neutron-scattering measurements, made using the Multi Angle Rotor Instrument (MARI) time-of-flight spectrometer at the Rutherford Laboratory, give information about the excitation spectrum as a function of wave vector transfer across the Brillouin zone. As well as studying the one-dimensional phase, we have investigated the effects of three-dimensional ordering on magnetic excitations to the first excited states.

The rest of the paper is organized as follows: The next section describes the chemical and magnetic structures. Section III outlines the theory and derives the modifications to the spin Hamiltonian. The new neutron experiment is described, and results presented in Secs. IV and V, respectively. A critical comparison of the data with this and previous theories is made in Sec. VI, and finally, conclusions are drawn in Sec. VII.

II. STRUCTURE AND MAGNETIC ORDERING IN $CsCoCl_3$

The crystal structure of $CsCoCl_3$, which is hexagonal with space group $P6_3/mmc$, is shown in Fig. 1. There are two formula units per unit cell, and the lattice parameters at a temperature $T=25$ K are $a=7.14$ and $c=6.00$ Å.[15] The magnetic Co^{2+} ions are surrounded by trigonally distorted octahedra of Cl^- ions, and form chains along the c axis with successive octahedra sharing a common face.

The shared Cl^- ions provide a strong antiferromagnetic superexchange path between adjacent Co^{2+} ions within the chains. In contrast, Co^{2+} ions in adjacent chains are separated by large Cs^+ ions, and because of the large distance between chains and the more complicated exchange paths, the antiferromagnetic exchange coupling between ions in neighboring chains is some two orders of magnitude weaker. This accounts for the quasi-one-dimensional magnetic behavior of $CsCoCl_3$.

The $(CoCl_3)^-$ chains are stacked, with Cs^+ ions between, into a triangular array. Because the exchange coupling between chains is antiferromagnetic, this triangular array forms a frustrated system. Two three-dimensionally ordered phases occur in $CsCoCl_3$. First, below $T_{N1}\sim 21$ K, a partially disordered antiferromagnetic "A phase" is formed in which one-third of the chains are paramagnetic. Then a further phase change takes place below $T_{N2}\sim 10$–14 K to a ferrimagnetic "F phase" where the remaining paramagnetic

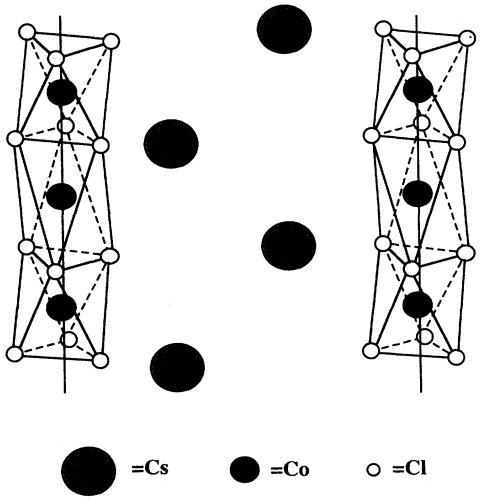

FIG. 1. The chemical structure of $CsCoCl_3$, showing the chains of Co^{2+} ions, coordinated by trigonally distorted octahedra of Cl^- ions. In the one-dimensional magnetic phase the spins on the Co^{2+} ions align antiferromagnetically along the hexagonal c axis.

chains align in the same direction, so that 2/3 of the chains are aligned in one way and 1/3 in opposition; see Fig. 2.[16] A nearest-neighbor interaction cannot explain this ordering, and a weak next-nearest-neighbor ferromagnetic interaction has been proposed to account for the ordered phases.[2]

III. THEORY

The spin dynamics of $CsCoCl_3$ requires careful consideration of crystal-field states of the Co^{2+} ions and their behavior as a many-body system when exchange coupled in a chain. In the first part of this section we consider the crystal-field states of isolated ions. This is followed by a discussion of the many-body spin Hamiltonian which, as usual, is derived as a projection of the exchange into the lowest Kramers doublet. Perturbation from the pure Ising limit gives rise to a continuum of soliton-pair states for isolated chains, which may be split into discrete levels by interactions with adjacent chains.[1,2] Finally we argue that the exchange mixing with higher single-ion levels of the same order of perturbation must be included.

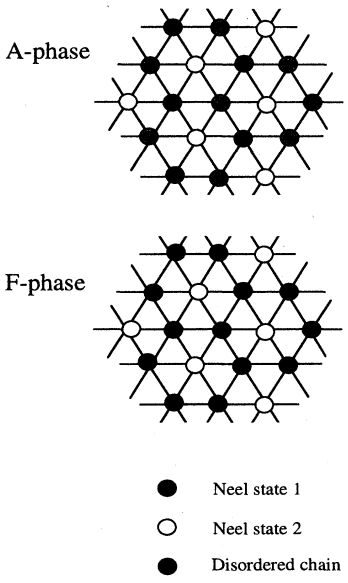

FIG. 2. The magnetic structure in the ab plane in the three-dimensionally ordered phases. For clarity only the Co^{2+} chains are shown.

A. Crystal field

According to Hund's rules the lowest-lying state of the free Co^{2+} ion is ^4F. The effects on the Co^{2+} ion of a strong cubic crystal field with a small trigonal distortion are well documented.[17,18] A cubic crystal field splits the lowest-lying multiplet into two orbital triplets and an orbital singlet, with a triplet lowest by some 890 meV. The lowest $^4T_1$ triplet has the same symmetry as a manifold of P states and can be described as an effective $L=1$ state. The cubic crystal field causes a small admixture of this state with a much higher free-ion ^4P term.

The trigonal distortion and spin-orbit coupling split the ground state into six Kramers doublets. These may be introduced in the perturbing single-ion Hamiltonian[18]

$$H^{\mathrm{SI}}=-\tfrac{3}{2}k\lambda\mathbf{L}\cdot\mathbf{T}-\delta(L_z^2-\tfrac{2}{3}), \tag{1}$$

where $\mathbf{T}$ is the true spin, L is the effective orbital angular momentum, λ is the spin-orbit coupling constant, and δ is the trigonal distortion parameter. Allowance is made for covalency and the small admixture of levels by the constant k, which is less than but of order unity.

The exchange interaction between true spins is given by

$$H^{\mathrm{ex}}=\sum_i I\mathbf{T}_i\cdot\mathbf{T}_{i+1}, \tag{2}$$

where $\mathbf{T}_i$ is the true spin vector on the ith site and I is the isotropic Heisenberg exchange. This may be regarded as a molecular field, and lifts the degeneracy of the Kramers doublets. The energies of electronic excitations, measured using inelastic neutron-scattering techniques, have enabled $k\lambda$, δ, and I to be determined.[19] The energies of the Co^{2+} ion in $CsCoCl_3$ are presented schematically in Fig. 3.

B. Ising-like model

The usual method for considering the exchange coupling between Co^{2+} ions in $CsCoCl_3$ is to project the Heisenberg interaction between true spins into the lowest-lying Kramers doublet,[9]

$$\Psi_{+1}(j^z=1/2)=c_1|-1,3/2\rangle+c_2|0,1/2\rangle+c_3|1,-1/2\rangle,$$
$$\Psi_{-1}(j^z=-1/2)=c_1|1,-3/2\rangle+c_2|0,-1/2\rangle+c_3|-1,1/2\rangle. \tag{3}$$

This leads to an effective $S=\frac{1}{2}$ Hamiltonian with anisotropic exchange,

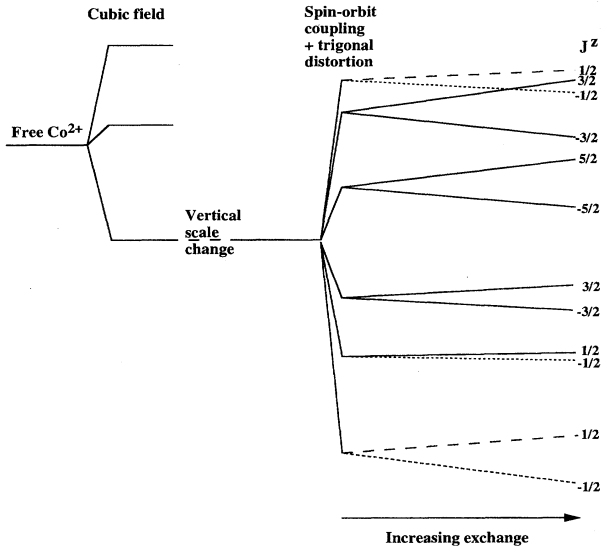

FIG. 3. Schematic diagram of the crystal-field levels of the Co^{2+} ion in $CsCoCl_3$ (Ref. 19). Spin-orbit coupling gives rise to a mixing of levels with the same $J^z=L^z+T^z$.

$$H=2J\sum_i [S_i^z S_{i+1}^z+\epsilon(S_i^x S_{i+1}^x+S_i^y S_{i+1}^y)], \tag{4}$$

where J is the effective intrachain exchange and

$$\epsilon=2(c_2^2+\sqrt{3}c_1c_3)/(3c_1^2+c_2^2-c_3^2). \tag{5}$$

The approach used to find the first excited states of the Ising-like Hamiltonian is to use the Ising basis and treat $\epsilon(\sim 0.1)$ as a perturbation.[1] In the pure Ising limit there are two degenerate ground states and a highly degenerate set of first excited states of energy $2J$. These are obtained by reversing a block of ν adjacent spins, as shown in Fig. 4. If ν is odd, the change in total spin $\Delta S^T=\pm 1$; if it is even, there is no change. In the momentum representation the basis states for $\Delta S^T=1$ may be written in terms of the spin-flip creation and annihilation operators

$$\Psi_1(Q)=\sqrt{\frac{2}{N}}\sum_i e^{iQR_i}S_i^+\Psi_{\text{Néel 1}},$$

$$\Psi_3(Q)=\sqrt{\frac{2}{N}}\sum_i e^{iQR_i}S_i^+S_{i+1}^-S_{i+2}^+\Psi_{\text{Néel 1}},$$

$$\cdots$$

$$\Psi_3(Q)=\sqrt{\frac{2}{N}}\sum_i e^{iQR_i}S_i^+\prod_{\nu=1}^{(N/2)-1}(S_{i+2\nu-1}^-S_{i+2\nu}^+)\Psi_{\text{Néel 1}}. \tag{6}$$

These are the domain wall (soliton) pair states moving with center-of-mass wave vector Q on a chain of N ions. $\Psi_1(Q)$ and $\Psi_{N-1}(Q)$ are spin-wave states since they are single-spin deviations from the fully aligned Néel states. The transverse coupling $\epsilon(S^xS^x+S^yS^y)$ lifts the degeneracy of the first excited states, and allows the solitons to become mobile. This gives rise to a continuum of excited states (see Fig. 5) with bounds given by

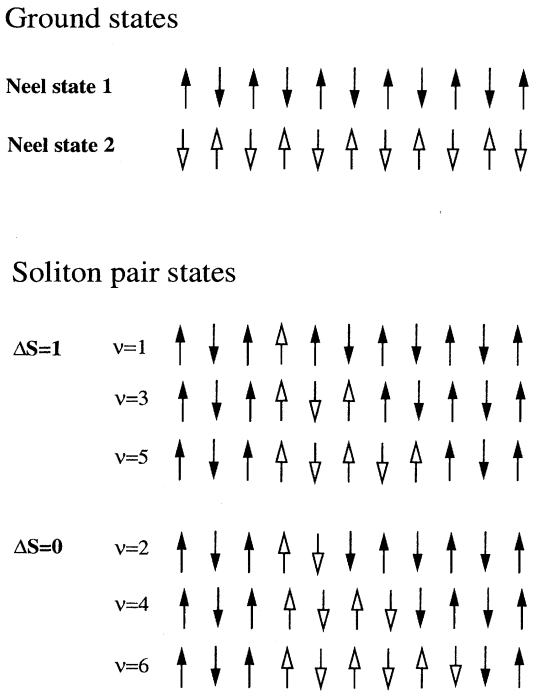

FIG. 4. The ground and first excited states in the pure Ising limit. A soliton-pair state is obtained from a Néel state by reversing a block of ν spins.

$$\omega^{\pm}=2J(1\mp 2\epsilon\cos Q), \tag{7}$$

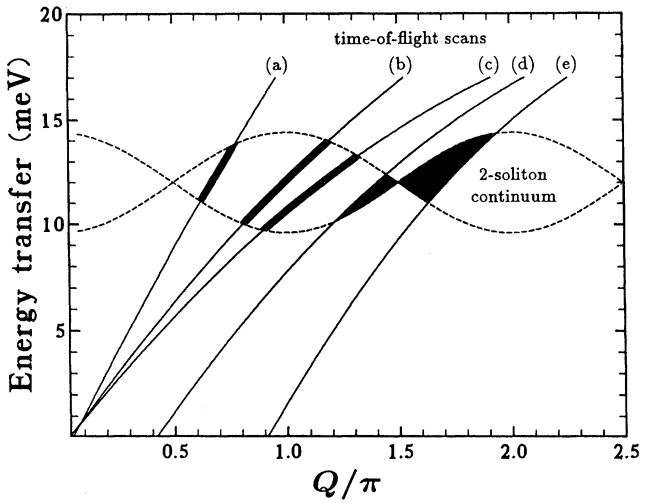

FIG. 5. Schematic diagram of the continuum of first excited states. The bounds of the continuum (dashed lines) may be calculated using Eq. (7). The solid lines show the scattering trajectories for MARI scans where (a) $E_0=50$ meV, $\bar{\phi}=8°$, (b) $E_0=25$ meV, $\bar{\phi}=8°$, (c) $E_0=20$ meV, $\bar{\phi}=8°$, (d) $E_0=20$ meV, $\bar{\phi}=30°$, and (e) $E_0=20$ meV, $\bar{\phi}=45°$. The highlighted (black) regions show where magnetic scattering is expected.

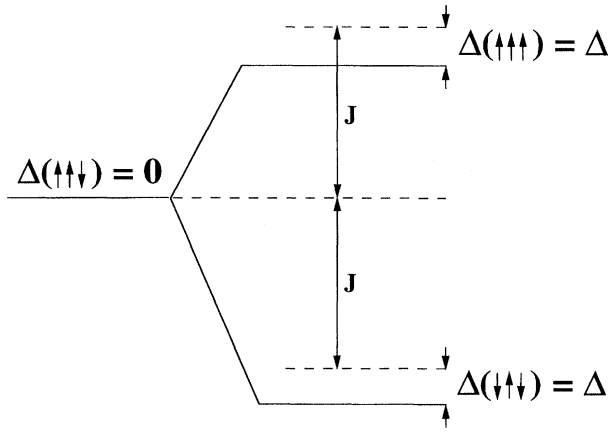

FIG. 6. The calculated splitting of the lowest Kramers doublet is shown as a solid line, and the symmetric splitting assumed in the absence of exchange mixing with higher levels is shown as a dashed line.

where Q is the one-dimensional wave vector transfer.

In the three-dimensionally ordered phases it is necessary to include an additional term

$$H^{\mathrm{IC}}=h^{\mathrm{IC}}\sum_i (-1)^i S_i^z, \tag{8}$$

where

$$h^{\mathrm{IC}}=2J^{\mathrm{IC}}\sum_j \langle S_{ij}^z\rangle, \tag{9}$$

and J^{IC} is the interchain exchange and the summation is over nearest-neighbor chains. This causes decoupling of the soliton-pair states and leads to quantization of the excitation continuum into a "Zeeman ladder" of excited states.[2]

C. Exchange mixing

In order to calculate the electron energy levels of the Co^{2+} ion in $CsCoCl_3$ it is necessary to diagonalize the following 12×12 Hamiltonian:

$$H^{\mathrm{SI}}=-\tfrac{3}{2}k\lambda\mathbf{L}\cdot\mathbf{T}-\delta(L_z^2-\tfrac{2}{3})+H_mT^z, \tag{10}$$

where T is the true spin $\frac{3}{2}$, $L=1$, and H_m is the molecular field. The off-diagonal terms in the spin-orbit interaction give rise to a mixing of levels with the same $J^z=L^z+T^z$. The spin-orbit and trigonal distortion parameters determined using inelastic neutron scattering are $k\lambda=18.4$ meV and $\delta=51.3$ meV.[19] The molecular field may then be adjusted to give the known splitting $2J=13$ meV of the ground state. Rather than the symmetric splitting of the ground state assumed in the Ising-like model, the effect of the mixing with higher levels is found to be depression of both levels by the same amount Δ; see Fig. 6. In fact, this can also be seen qualitatively using nondegenerate second-order perturbation theory, where the first-order term gives symmetric splitting and the squared second-order term gives a depression of both levels.

The molecular fields from nearest neighbors experienced by individual Co^{2+} ions in chains containing soliton-pair states are of three types. These are $\uparrow\uparrow\downarrow$ where the central ion is in zero molecular field, $\downarrow\uparrow\downarrow$ which corresponds to the lowest level in the molecular field, and $\uparrow\uparrow\uparrow$ which is the first excited state in the molecular field. If the mixing of higher states is neglected the spin states $\uparrow\uparrow\uparrow$ and $\downarrow\uparrow\downarrow$ split symmetrically about $\uparrow\uparrow\downarrow$. Including the mixing we must change the energies of the states by $\Delta(\uparrow\uparrow\downarrow)=0$ and $\Delta(\uparrow\uparrow\uparrow)=\Delta(\downarrow\uparrow\downarrow)=\Delta$. When the solitons are separated the energy difference between neglecting mixing and including it for a chain of N ions is

$$E^{\mathrm{SEP}}=N\Delta(\downarrow\uparrow\downarrow)-4\Delta(\downarrow\uparrow\downarrow)+4\Delta(\uparrow\uparrow\downarrow). \tag{11}$$

If, on the other hand, the solitons are adjacent, there will be an $\uparrow\uparrow\uparrow$ state and the energy difference is

$$E^{\mathrm{ADJ}}=N\Delta(\downarrow\uparrow\downarrow)-3\Delta(\downarrow\uparrow\downarrow)+2\Delta(\uparrow\uparrow\downarrow)+\Delta(\uparrow\uparrow\uparrow). \tag{12}$$

Thus the spin-wave states differ in energy from the other two-soliton states by

$$E^{\mathrm{SEP}}-E^{\mathrm{ADJ}}=-(\Delta(\uparrow\uparrow\uparrow)+\Delta(\downarrow\uparrow\downarrow))=2\Delta. \tag{13}$$

For self-consistency it is necessary to consider how the mixing of levels modifies the spin T^z, since this will alter the molecular field experienced by neighboring ions, and in turn modify the field at the original ion. The molecular field is given by $H_m=2J\Sigma_i\langle T_i^z\rangle$ where the summation is over the two neighboring ions in the chain. It is assumed in the first calculation that for ions in the sequence $\ldots\downarrow\uparrow\uparrow\uparrow\downarrow\ldots$ the central ion experiences a molecular field and the two adjacent ions do not. The diagonalization of Eq. (10) yields the wave functions [Eq. (3)] and hence the new value of $T^z=\frac{3}{2}c_1^2+\frac{1}{2}c_2^2-\frac{1}{2}c_3^2$ for this site. Since the molecular fields at the neighboring sites no longer cancel, the new wave functions at these sites must be calculated. The spins T^z derived for these sites are then used to recalculate the molecular field at the original site. When this calculation is performed iteratively convergence is rapid and the levels are only slightly modified. The final value obtained is $\Delta=0.09J$.

Thus we propose a spin Hamiltonian for the lowest two states with diagonal terms so that

$$\langle\nu,Q|H|\nu,Q\rangle=\begin{cases}2J+h^{\mathrm{IC}}\nu, & \nu=1,N-1,\\ 2J+h^{\mathrm{IC}}\nu+2\Delta, & \text{otherwise,}\end{cases}$$

and off-diagonal terms

$$\langle\nu,Q|H|\nu',Q\rangle=\begin{cases}J\epsilon[1+e^{2iQ}], & \nu'=\nu-2,\\ J\epsilon[1+e^{-2iQ}], & \nu'=\nu+2,\\ 0, & \text{otherwise,}\end{cases} \tag{14}$$

where ν runs over the values $1,3,5,\ldots,N-1$.

D. Neutron scattering

The inelastic neutron-scattering cross section is given by[20]

$$\frac{d^2\sigma}{d\Omega d\omega}\propto|f(Q)|^2\sum_{\alpha\beta}(\delta_{\alpha\beta}-Q_\alpha Q_\beta)S^{\alpha\beta}(\mathbf{Q},\omega), \tag{15}$$

where $\mathbf{Q}$ is the total wave vector transfer and $f(Q)$ is the magnetic form factor. The dynamic response is the Fourier transform in space and time of the the dynamic two-spin correlation function

$$S^{\alpha\beta}(\mathbf{Q},\omega)=\frac{1}{2\pi}\sum_j e^{i\omega t}e^{iQj}\langle S_0^{\alpha}(0)S_j^{\beta}(t)\rangle dt. \quad (16)$$

For our effective spin Hamiltonian the ground state $|G\rangle$ is given to first order by

$$|G\rangle=|\Psi_{\text{Néel 1}}\rangle+\frac{1}{E_N-H_I}H|\Psi_{\text{Néel 1}}\rangle, \quad (17)$$

where $|\Psi_{\text{Néel 1}}\rangle$ is one of the two Néel states of the Ising Hamiltonian H_I, and E_N is the Néel state energy. The first excited states $|E\rangle$ are found by diagonalizing Eq. (14) and periodic boundary conditions are assumed. The scattering is dominated by the transverse response[1] $S^{xx}(\mathbf{Q},\omega)$ which is calculated using

$$S^{xx}(\mathbf{Q},\omega)=\sum_E |\langle E|S_Q^x|G\rangle|^2\delta(\omega-E), \quad (18)$$

where

$$S_Q^x=\frac{1}{\sqrt{N}}\sum_j e^{iQj}S_j^x. \quad (19)$$

IV. EXPERIMENTAL PROCEDURE

A single crystal of $CsCoCl_3$ was grown using the Bridgeman technique by Dr. R. C. C. Ward of the Clarendon Laboratory. In order to minimize the effects of neutron absorption, a smaller approximately right cylindrical fragment roughly 1 cm^3 in volume was cleaved from the boule. The sample was mounted in an orange cryostat at the position of the center of rotation of MARI, which is situated on the ISIS pulsed neutron facility at the Rutherford Laboratory.

The inelastic neutron spectrometer MARI uses a Fermi chopper to obtain monochromatic neutrons of incident energy E_0 in the range 10–2000 meV. The scattered neutrons are detected in a low angle ($\phi=3.86°-12°$) array of eight banks of ^{3}He detectors arranged symmetrically about the direction of the incident beam, and in a high-angle array of detectors covering scattering angles up to $\phi=135°$.[21] The spectra are corrected for detector efficiencies and are normalized for solid-angle coverage by measuring the scattering from a vanadium standard. Monochromatic vanadium scans are used to correct for the transmission of the chopper. The data are acquired as time of flight and are converted to units of energy transfer (meV). The data have also been corrected for the kinematical factor k_f/k_i and have a well-characterized background subtracted. In this experiment most of the measurements were carried out at relatively low incident energies E_0 = 20 and 25 meV, to take advantage of the narrow intrinsic resolution, which is roughly 2% of E_0.

MARI is particularly well suited to the study of one-dimensional magnetic systems. Good counting statistics may be achieved by mounting the crystal with the chain direction parallel to the incident beam, since in this case the detectors in the low-angle bank give identical information and can be summed without loss of information. Furthermore, the higher-angle detectors simultaneously probe the wave vector dependence of the scattering, and so the magnetic origin of the scattering may be confirmed by following it out to higher Q and comparing with the predicted magnetic form factor dependence. This procedure also checks for the possibility of phonon contamination.

For a fixed scattering angle ϕ, both the wave vector and energy transfer vary with time of flight, so that experiments record data along lines in Q, E space, as shown in Fig. 5. The reduced magnetic scattering vector parallel to the chain direction may be expressed as

$$Q_{\parallel}=\frac{c}{2}\{\gamma[E_0(1+\cos^2\phi-2\cos\phi\sqrt{1-\omega/E_0}) -\omega\cos^2\phi]\}^{1/2}, \quad (20)$$

where the constant $\gamma=0.4826$ Å^{-2} meV^{-1}. The scattering locus $(Q_{\parallel},E)$ of scans taken in the low-angle bank with $\bar{\phi}=8°$ and $E_0=50$, 25, and 20 meV are presented in Figs. 5(a), 5(b), and 5(c), respectively. This diagram also shows schematically the continuum of first excited states. The highlighted (black) regions show where the loci intersect the excitation continuum, and magnetic scattering is expected. The loci (d) and (e) show the extremes ($\phi=$ 30° and 45°) of a higher-angle group of detectors for E_0 = 20 meV. This region covers the important area in the vicinity of the zone boundary.

V. RESULTS

In all of our measurements broad scattering from the continuum of first excited states was detected in the low-angle bank; see, for example, Fig. 7. This feature occurs between energy transfers in the range 10–16 meV, as expected.[7,11] The magnetic origin of this component has been confirmed by following the scattering out to higher Q in the higher-angle detectors. Since the intensities of the various components of the scattering do not grow systematically with either scattering vector or temperature, it is deduced that the neutron spectra presented below are free from phonon contamination.

The data acquired in the low-angle bank of detectors with an incident energy $E_0=25$ meV [see Fig. 5(b)] are presented as a function of temperature in Fig. 7. In each case the background, measured using the empty cryostat, has been subtracted. In the one-dimensional phase at $T=25$ K the measurements clearly show an asymmetry of the excitation continuum, with the scattering biased toward lower energies. Discrete lines appear in the three-dimensionally ordered phases at $T=17$ and 2 K, which correspond to the A and F phases, respectively. Figure 8 shows the scattering in the simplest three-dimensional phase at $T=2$ K elsewhere in the Brillouin zone; Fig. 8(a) corresponds to the region between Fig. 5(d) and 5(e), 8(b) to 5(a), and 8(c) to 5(c). Near the Brillouin zone boundary [Fig. 8(a)] the width in energy transfer is seen to narrow.

The scattering function $S(Q_{\parallel},\omega)$ has been calculated numerically using the new theory. In the one-dimensional phase the interchain coupling h^{IC} is zero, but in the A phase h^{IC} = 0, $2J^{\text{IC}}$, $4J^{\text{IC}}$, and $6J^{\text{IC}}$ in the proportions 5/12, 3/12, 3/12, and 1/12, and in the F phase the weighting for h^{IC} = 0 and

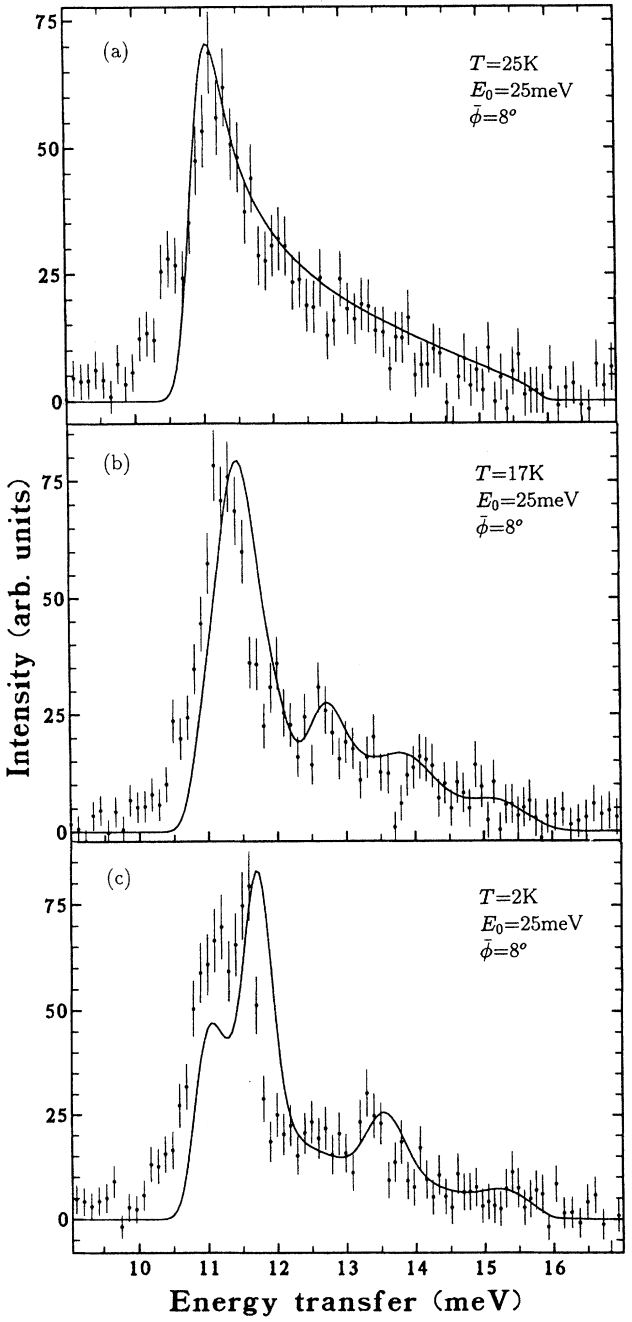

FIG. 7. Neutron spectra measured in the low angle bank with $\bar{\phi}=8°$ and $E_0=25$ meV [see Fig. 5(b)] as a function of temperature. Asymmetric continuum scattering is observed at $T=25$ K (a) in the one-dimensional phase, and discrete lines appear at $T=17$ K (b) and 2 K (c) in the A and F phases, respectively. The solid line shows the scattering calculated with the exchange mixing model, using Eq. (14).

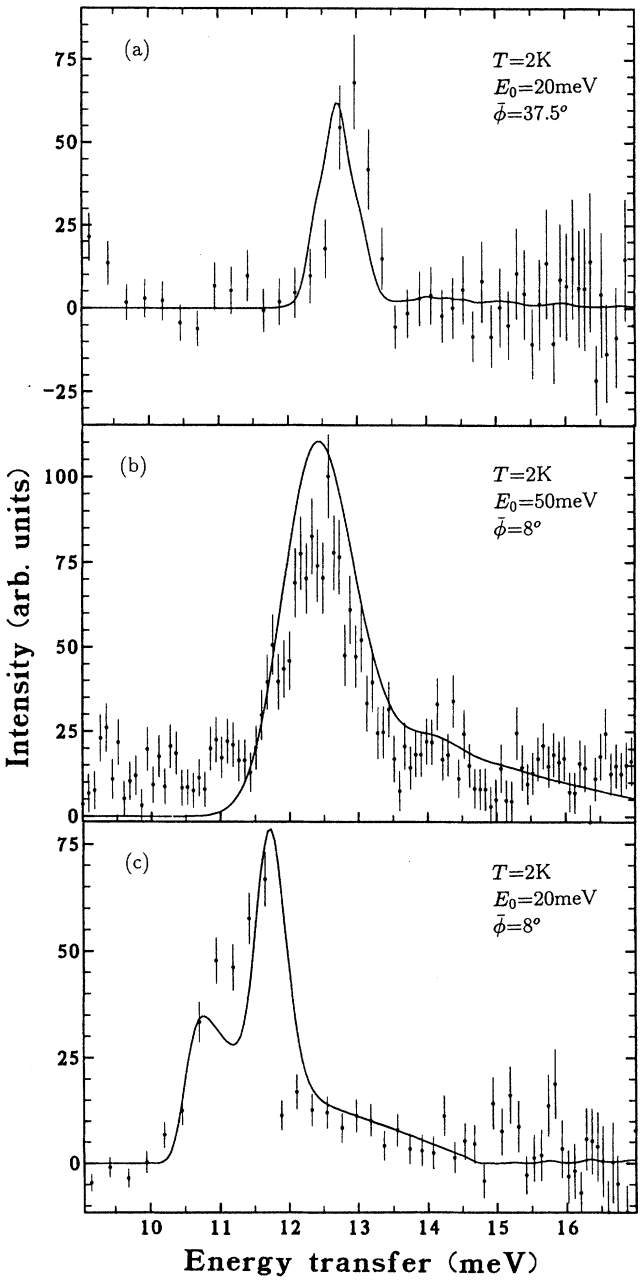

FIG. 8. The model is compared with neutron measurements at $T=2$ K elsewhere in the Brillouin zone: (a) near the zone boundary between 5(d) and 5(e); (b) 5(a); (c) 5(c).

$6J^{IC}$ is 2/3 and 1/3. The eigenstates and eigenvalues were obtained by diagonalizing the Hamiltonian in Eq. (14). Here we have used chains of $n=80$ spins throughout; no change can be discerned for n above 40.

In order to reproduce the observed $S(Q_{\parallel},\omega)$ the calculation was performed over the scattering locus defined by Eq. (20). The results were convolved with the instrumental energy resolution function, which may be approximated by a Gaussian with full width half maximum (FWHM) uniquely determined by the ratio ω/E_0.[22] The solid lines in Figs. 7 and 8 show the calculated scattering, corrected for magnetic form factor $\langle j_0 \rangle$ (Ref. 23) and polarization factor [Eq. (15)].

Although there is an arbitrary overall scale factor, the different scans have been normalized consistently so that intensities can be compared directly. There are small discrepan-

cies between the calculated and measured spectra, particularly at low energies where the scattering tends to be underestimated. However, a model in which $J=6.37$ meV, $\epsilon=0.145$, $J^{IC}=0.008J$, and $\Delta=0.11J$ accounts adequately for the neutron data at all temperatures and across the Brillouin zone. In Fig. 7(a) we see that the model successfully predicts the line shape of the continuum scattering, and in Figs. 7(b) and 7(c) the appearance of discrete lines in the A and F phases. As shown in Fig. 8 the form of the scattering is correct elsewhere in the Brillouin zone, narrowing at the zone boundary [Fig. 8(a)]. Furthermore, the experimental value of Δ is within 20% of the theoretical value calculated in Sec. III C.

VI. DISCUSSION

In order to explain the disprepancies between theory and observations on the experimental realizations of Ising-like systems, the $MCoX_3$ salts, a variety of explanations have been proposed. There seems to be no physical justification for the models in which the anisotropy[7] or the interchain exchange[8] are allowed to vary for each of the series of Raman lines. Furthermore, these theories are unable to explain the sharp onset of the continuum scattering at low energies. More recently authors have considered exchange mixing[11] and next-nearest-neighbor (NNN) intrachain coupling,[14] but neither approach has been entirely successful.

In the first attempt to take account of exchange mixing an effective Hamiltonian was proposed, which includes a slow internal staggered field.[11] The main theoretical objection to this approach is that it is essentially a mean field theory, which assumes that the neighboring ions are in a Néel state. This works in higher dimensions where spin waves are the basic excitations,[24] but it is inappropriate when applied to the soliton-pair states discussed here. Although this model gives enhanced scattering at low energies, it predicts another series of lines rather than the continuous spectrum observed, particularly in the Raman measurements which have very high resolution.[7]

It is possible to obtain continuum scattering with a peak at low energy and a tail at higher energies if NNN coupling is included.[14] In order for NNN coupling to explain the results a ferromagnetic NNN exchange of magnitude $|J^{NNN}|\sim 0.1|J|$ is required,[14] which considering that the NNN exchange is through two nonmagnetic ligands would seem to be unphysically large. However, the proposed form for NNN coupling gives a good description of most of the experimental data. The main consequence of including a NNN term is to distinguish energetically between a spin-wave state and the other two-soliton states. Yet we have shown in Sec. III C that this is precisely what the correct treatment of exchange mixing does.

In Fig. 9 the results of our neutron-scattering investigation are compared with the predictions of the previous theories. The scans recorded in the low-angle bank of detectors with an incident energy $E_0=25$ meV [see Fig. 5(b)] which probe the region near $Q=\pi$ are shown for $T=25$ [Fig. 9(a)] and $T=2$ K [Fig. 9(b)], and the scattering in the vicinity of $Q=3\pi/2$ [between Figs. 5(d) and 5(e)] is shown for $T=2$ K [Fig. 9(c)]. The dashed line shows the form proposed for the slow internal staggered field,[11] and the dotted line shows the NNN model,[14] after convolution with the instrumental resolution function. The good resolution of these results clearly demonstrates the inability of the previous exchange mixing model to account for the data. On the other hand, it could be argued that the NNN model successfully reproduces the data

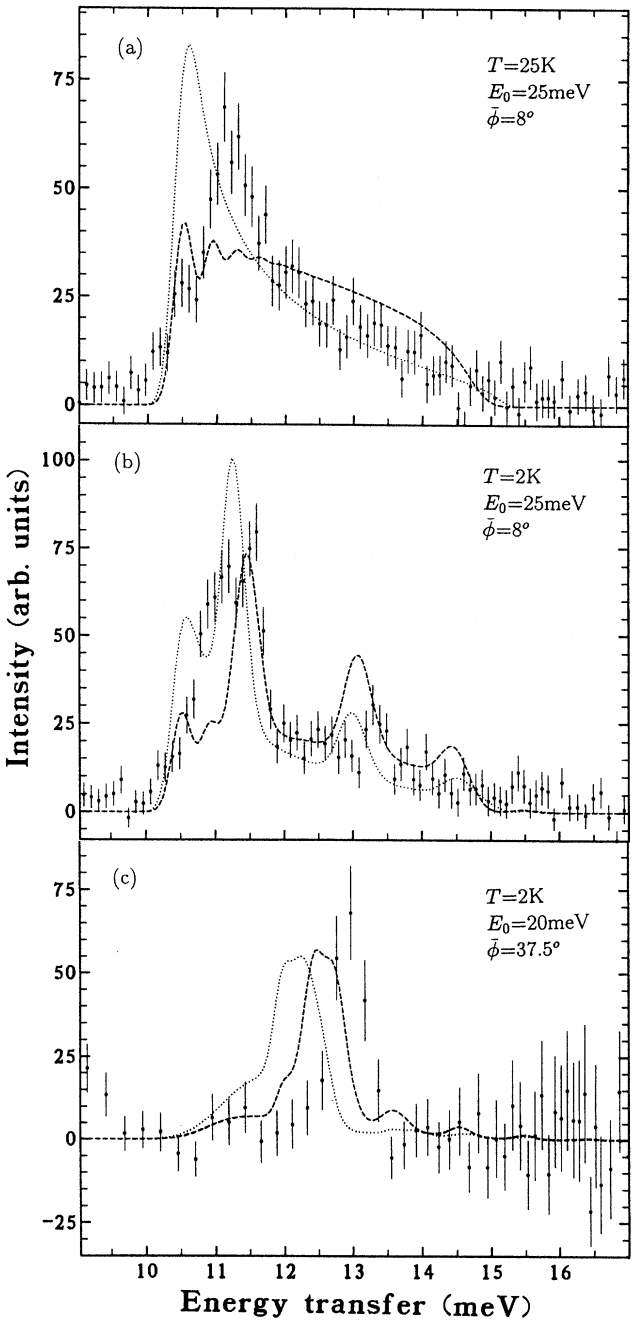

FIG. 9. Comparison of previous models with typical neutron results: (a) 5(b) at $T=25$ K; (b) 5(b) at $T=2$ K; (c) between 5(d) and 5(e) at $T=2$ K. The calculated scattering is shown as a dashed line for the slow internal staggered field (Ref. 11), and a dotted line for NNN intrachain coupling (Ref. 14).

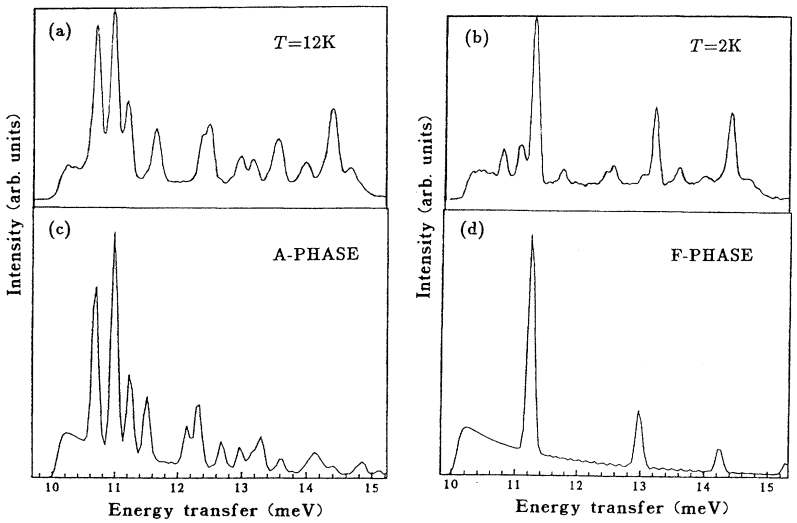

FIG. 10. Comparison of previous Raman measurements (Ref. 7) with $S^{xx}(Q=0,\omega)$ calculated using Eq. (14). Experimental data are shown (a) for $T=12$ K and (b) $T=2$ K, and simulations (c) for the ideal A phase and (d) F phase.

near $Q=\pi$, provided the energy scale is renormalized. However, the NNN term is dispersive and leads to an underestimation of the energy of the narrow feature near $Q=3\pi/2$, which cannot be explained even if the overall energy scale is modified. In contrast our neutron-scattering results are in quantitative agreement with the theory derived in Sec. III C.

The model is compared with the Raman-scattering results[7] in Fig. 10. Although, unlike neutron scattering, the precise matrix elements are unknown, it can be compared approximately with $S(Q,\omega)$ at $Q=0$, with very high resolution in ω. The simulations show $S^{xx}(Q=0,\omega)$ calculated using the Hamiltonian in Eq. (14), and convolved with the quoted instrumental energy resolution for the ideal ordered phases. In this calculation the overall energy scale has been reduced by 3.6% to take account of possible calibration errors. The model explains the Raman measurements at least as well as previous attempts. The main discrepancies are the intense feature near $E=14.5$ meV, which has been attributed to phonon contamination,[7] and the presence of small extra peaks at $T=2$ K, which coincide with strong peaks in the A phase. The latter features are readily understood in terms of domain boundaries.[2,14]

It seems reasonable to assume that the model described above should be employed to explain the Raman spectra from $RbCoCl_3$,[25] and the neutron[11] and Raman[7] results from $CsCoBr_3$, since these are qualitatively similar to those from $CsCoCl_3$. It should also be used when the above systems are doped with nonmagnetic ions, such as $CsCo_xMg_{1-x}Cl_3$. The doping breaks up the chain, and as well as the two-soliton peak at $E\sim 2J$, there is a peak at $E\sim J$ associated with spins at the ends of the finite chains.[26] In fact, it has proved impossible to explain the Q dependence of the peak near $E\sim J$ using a dispersive NNN term.[27]

VII. CONCLUSIONS

We have derived a theory which properly takes account of the exchange mixing of higher levels in $CsCoCl_3$. The asymmetric splitting of the lowest Kramers doublet of the Co^{2+} ion in a molecular field leads to the conclusion that the spin-wave states are lower in energy than the other two-soliton states. This means that an extra exchange mixing term Δ must be incorporated in the effective spin Hamitonian. Using the time-of-flight neutron spectrometer MARI we have measured $S(Q,\omega)$ across the Brillouin zone, at higher resolution than before, and without contamination from phonon scattering. From our results we are able to deduce a value of Δ that is in quantitative agreement with the value calculated using the known crystal-field parameters. The theory is consistent with all of the available neutron and Raman data on $CsCoCl_3$, and so there is no evidence for a large next-nearest-neighbor intrachain interaction. These developments should also be taken into account when analyzing other pure and doped $MCoX_3$ systems.

ACKNOWLEDGMENTS

We would like to express our gratitude to R. A. Cowley for his help and advice and to R. C. C. Ward for the provision of an excellent sample. The expert technical assistance of the staff of the Rutherford Laboratory is gratefully acknowledged. In particular we thank T. G. Perring and R. S. Eccleston for help in running the spectrometer. Financial support was provided by the Engineering and Physical Science Research Council, and one of us (S.E.N.) received additional support from the U.S. Department of Energy under Grant No. DE-FG05-92ER45280.

*Present address: Department of Physics, Oak Ridge National Laboratory, Oak Ridge, TN 37831-6393.

[1] N. Ishimura and H. Shiba, Prog. Theor. Phys. **63**, 743 (1980).
[2] H. Shiba, Prog. Theor. Phys. **64**, 466 (1980).
[3] G. Muller, H. Thomas, H. Beck, and J. C. Bonner, Phys. Rev. B **24**, 1429 (1981).
[4] D. A. Tennant, T. G. Perring, R. A. Cowley, and S. E. Nagler, Phys. Rev. Lett. **70**, 4003 (1993).

[5] F. D. M. Haldane and M. R. Zirnbauer, Phys. Rev. Lett. **71**, 4055 (1993).
[6] T. Kohmoto, T. Goto, S. Maegawa, N. Fujiwara, Y. Fukada, M. Kunitomo, and M. Mekata, Phys. Lett. A **167**, 493 (1992).
[7] W. P. Lehmann, W. Breitling, and R. Weber, J. Phys. C **14**, 4655 (1981).
[8] I. W. Johnstone, D. J. Lockwood, and M. W. C. Dharma-Wardana, Solid State Commun. **36**, 1033 (1980).
[9] U. Tellenbach, J. Phys. C **11**, 2287 (1978).
[10] H. Yoshizawa, K. Hirakawa, S. K. Satija, and G. Shirane, Phys. Rev. B **23**, 2298 (1981).
[11] S. E. Nagler, W. J. L. Buyers, R. L. Armstrong, and B. Briat, Phys. Rev. B **27**, 1784 (1983).
[12] F. Matsubara and S. Inawashiro, Phys. Rev. B **41**, 2284 (1990).
[13] F. Matsubara and S. Inawashiro, Phys. Rev. B **43**, 796 (1991).
[14] F. Matsubara, S. Inawashiro, and H. Ohhara, J. Phys. Condens. Matter **3**, 1815 (1991).
[15] H. J. Seiffert, Z. Anorg. Allg. Chem. **307**, 137 (1961).
[16] M. Mekata and K. Adachi, J. Phys. Soc. Jpn. **44**, 806 (1978).
[17] A. Abragam and M. H. L. Pryce, Proc. R. Soc. London A **206**, 173 (1951).
[18] M. E. Lines, Phys. Rev. **131**, 546 (1963).
[19] T. Nguyen, S. E. Nagler, R. A. Cowley, T. Perring, and R. Osborn, J. Phys. Condens. Matter **7**, 2917 (1995).
[20] W. Marshall and S. W. Lovesey, *Thermal Neutron Scattering* (Clarendon, Oxford, 1971).
[21] *User Guide to the Experimental Facilities at ISIS*, edited by B. Boland and S. Whapham (Rutherford Appleton Laboratory, Didcot, UK, 1992).
[22] T. G. Perring, Ph.D. thesis, Cambridge University, 1991.
[23] P. J. Brown, in *International Tables for Crystallography C*, edited by A. J. C. Wilson (Kluwer, Dordrecht, 1995).
[24] W. J. L. Buyers, T. M. Holden, E. C. Svensson, R. A. Cowley, and M. T. Hutchings, J. Phys. C **4**, 2139 (1971).
[25] D. J. Lockwood, I. W. Johnstone, H. J. Labbe, and B. Briat, J. Phys. C **16**, 6451 (1983).
[26] S. E. Nagler, W. J. L. Buyers, R. L. Armstrong, and R. A. Ritchie, J. Phys. C **17**, 4819 (1984).
[27] K. Murao, F. Matsubara, and S. Inawashiro, J. Phys. Condens. Matter **4**, 2641 (1992).

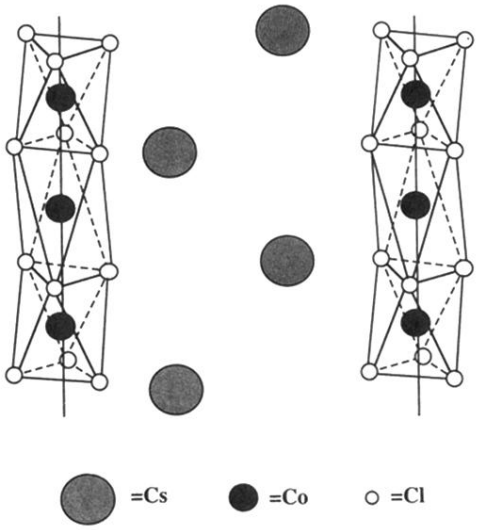

FIG. 1. The chemical structure of $CsCoCl_3$, showing the chains of Co^{2+} ions, coordinated by trigonally distorted octahedra of Cl^- ions. In the one-dimensional magnetic phase the spins on the Co^{2+} ions align antiferromagnetically along the hexagonal c axis.

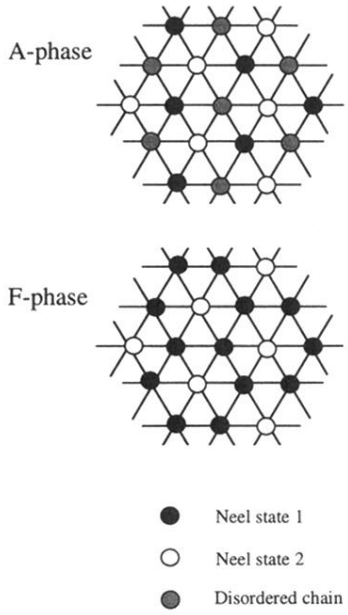

FIG. 2. The magnetic structure in the ab plane in the three-dimensionally ordered phases. For clarity only the Co^{2+} chains are shown.